International Journal of Heat and Mass Transfer 189 (2022) 122690

Contents lists available at ScienceDirect

International Journal of Heat and Mass Transfer

journal homepage: www.elsevier.com/locate/hmt

Analysis of thermophoresis for separation of polystyrene microparticles in microfluidic devices

Antton Sanjuan, Ane Errarte, M. Mounir Bou-Ali*

Mechanical and Manufacturing Department, Mondragon University, Loramendi 4, Apdo. 23, 20500 Mondragon, Spain

ARTICLE INFO

Article history:
Received 9 December 2021
Revised 24 January 2022
Accepted 7 February 2022
Available online 25 February 2022

Keywords:
Microparticles
Thermodiffusion
Thermophoresis
Microdevice and separation

ABSTRACT

We analysed the thermodiffusion phenomenon both numerically and experimentally for size-based separation of polystyrene microparticles. For model validation, we followed previously published numerical studies using ANSYS Fluent 2020 R2 software. For our experimental analysis, we defined a new microchannel geometry that would separate at least two groups of particles (5 and 20 μm). We analysed the trajectory of the microparticles in the central channel of the microdevice under the following conditions: without a temperature gradient, with application of a thermal gradient parallel to the gravitational field (cooling from the bottom or top part), and generation of a temperature gradient perpendicular to the direction of the gravity force. Numerical and experimental results for these geometry and boundary conditions demonstrated that, under terrestrial conditions, 5 μm and larger microsized polystyrene particles cannot be separated by thermophoresis in flow because of the gravity force.

1. Introduction

In recent years, the study of and interest in the phenomenon of thermodiffusion, discovered by C. Ludwig [1] and Ch. Soret [2] in the 19th century, has grown considerably [3]. Its applicability has spread to diverse unrelated areas, such as the characterisation of geological fields [4–6] or the sorting of biological species [7–9].

During the last few years, thermodiffusion has become a major interest in the health sector due to its involvement in transport in biological systems [10–12]. For example, the accumulation of biomolecules in thermophoretic traps has been achieved by combining thermodiffusion and convection [13]. Changes in the thermophoretic responses of a protein when a ligand is bound have also been analysed [14]. Moreover, thermodiffusion influences the process called Sperm Thermotaxis, which affects the transfer of sperm towards the direction of the egg [15]. The manipulation of DNA has also been carried out by light-induced local heating [16].

Thermodiffusion has now become a meaningful parameter in the microfluidic sector for optimisation of different separation processes [8,9,17], such as size-based nanoparticle species separation [18–20]. In the context of miniaturisation in the field of biotechnology, microscale sorting of biological cells is of great importance for the early diagnosis of diseases [21]. Nevertheless, in some of the analysed work, due to the time expenditure and complexity of the experimental trials, numerical results have frequently been shown without experimental validations [19,20].

Thermodiffusion, or the Ludwig-Soret effect, describes the mass transport of a mixture's components in the presence of a temperature gradient. The Soret (S_T) coefficient is the magnitude that represents this migration, and it depends on the thermodiffusion (D_T) and diffusion (D) coefficients of the components of the system. In binary mixtures, it is expressed by Eq. (1) [22].

$$S_T = \frac{D_T}{D} \tag{1}$$

In mixtures, depending on the direction of displacement of the densest component, the Soret coefficient can be positive or negative. When the densest species moves towards the cold side, the Soret coefficient is positive, designating the mixture as thermophobic. Otherwise, in a less common scenario, when the densest component migrates to the hot side, the coefficient is negative, naming the mixture as thermophilic.

Suspended particles will move towards the cold or hot zone, depending on the sign of the thermodiffusion coefficient, and they travel at a uniform velocity expressed by Eq. (2) [23]:

$$V_{T,i} = -D_{T,i}\nabla T \tag{2}$$

where ∇T is the spatial temperature gradient over the mixture and $V_{T,i}$ is the thermophoretic velocity of the component i. This dis-

* Corresponding author.
E-mail address: mbouali@mondragon.edu (M.M. Bou-Ali).

https://doi.org/10.1016/j.ijheatmasstransfer.2022.122690

Table 1
Defined boundary conditions by Eslamian et al. [24].

Boundary	Type	Values
Inlet	Velocity Inlet	$V = 1{\cdot}10^{-3}$ m/s $V_P = 1{\cdot}10^{-3}$ m/s
Upper and bottom outlet	Pressure Outlet Particle Scape	P gauge = 0 Pa
Hot wall (bottom part)	No-slip Particle Reflection	$T = 310$ K $e_n = 1.0$ (default)
Cold wall (upper part)	No-slip Particle Reflection	$T = 300$ K $e_n = 1.0$ (default)
Other walls	No-slip and Adiabatic Particle Reflection	$-k\nabla T = 0$ $e_n = 1.0$ (default)

placement of particles caused by thermal gradients is referred to as thermophoresis [18].

Considering that most of the published literature shows analyses of the effect of thermodiffusion on particle separation, the motivation for the present work was to study the possibility of classifying microparticles of different sizes based on thermal gradients.

In this work, we analysed the effect of thermodiffusion on the separation of polystyrene (PS) microparticles of different sizes (5 and 20 μm) in a microdevice. We first defined, validated, and analysed a numerical model based on the scientific work found in the literature. We then verified, both numerically and experimentally, the size-based separation of PS microparticles under a temperature gradient.

2. Numerical analysis and model validation

We analysed two different scientific papers that had studied the effect of thermodiffusion as a new method for the separation of microparticle species [24,25]. We used ANSYS Fluent 2020 R2 software for our analysis.

The governing equations of the process, together with the working conditions and the forces acting on the suspended particles, are described below.

2.1. Governing equations

We resolved both simulations using the Euler-Lagrange method, where we defined the fluid as the continuous phase and the dissolved particles in it as the secondary stage. We specified a laminar flow for the carrier fluid, and we tracked the suspended particles using the Discrete Phase Model (DPM) [26,27].

The mathematical expressions of mass, momentum and energy conservation laws for an incompressible steady-state fluid are the following [19,28]:

$$\nabla \cdot \vec{V} = 0 \tag{3}$$

$$\left(\vec{V} \cdot \nabla\right) \vec{V} = -\frac{1}{\rho}\nabla p + \nabla \cdot \left(\nu \nabla \vec{V}\right) \tag{4}$$

$$\nabla \cdot \left(\vec{V} c_p T\right) = \nabla \cdot \left(\frac{k}{\rho}\nabla T\right) \tag{5}$$

where $\vec{V}$ is the fluid velocity, ρ is the mixture density, ν is the kinematic viscosity and k and c_p correspond to the thermal conductivity and specific heat, respectively. T and p represent the temperature and pressure, respectively.

We also considered the temperature-dependant density changes in the fluid using the ANSYS Fluent Boussinesq model Eq. (6) [26]:

$$\rho = \rho_0(1 - \alpha(T - T_0)) \tag{6}$$

where ρ_0 is the initial density, α the thermal expansion coefficient and T_0 the initial temperature.

We accounted for the forces acting on the PS microparticles by considering gravity and drag, together with the thermophoretic force. In these conditions, the thermophoretic force represents the thermodiffusion phenomenon, and in fluent is defined by Eq. (7) [24]:

$$D_{T-F,\ i} = 6\pi\ T\ \mu\ R_i\ D_{T,i} \tag{7}$$

where μ is the dynamic viscosity of the fluid, R_i the radius of the particles of species i and $D_{T,i}$ is the experimental thermodiffusion coefficient of each particle group i, defined as Eq. (8) for binary mixtures:

$$\overrightarrow{J_i} = -\rho D \nabla c_i - \rho D_{T,i} c_i\ (1 - c_i)\nabla T \tag{8}$$

where $\overrightarrow{J_i}$ is the mass flux of the species i over the mixture, c_i is the concentration of the component i and ∇c_i the spatial gradient of mass fraction of the species i.

From Eq. (7), the numerical model calculates the value of the thermophoretic force acting on the particles by Eq. (9) [27], where $m_{p,i}$ is the mass of the particles of species i:

$$\overrightarrow{f_{T,i}} = -D_{T-F,i}\frac{1}{m_{p,i}T}\nabla T \tag{9}$$

Based on all these forces, Fluent determines the trajectory of the particles using the mathematical statement of motion Eq. (10) [27] and calculates the position of each particle along the channel. The program first solves the continuous phase and then resolves the particle injection. For that purpose, apart from the properties mentioned above, the drag force per unit particle mass $f_{drag}(\vec{V} - \vec{V}_p)$, gravity ($g$) and particle density ($\rho_p$), together with their velocity ($\vec{V}_p$), are all considered.

$$f_{drag}\left(\vec{V} - \vec{V}_p\right) + \frac{g(\rho_p - \rho)}{\rho_p} + \overrightarrow{f_{T,i}} = d\frac{\vec{V}_p}{dt} \tag{10}$$

2.2. Case study 1: thermophoretic 1 μm particle separation in a rectangular T-shaped microchannel

Eslamian et al. [24] analysed the effect of thermodiffusion on the separation of polystyrene (PS) and gold microparticles in water and air. In the present work, we conducted an equivalent study using water as the carrier fluid and applying the same geometric, mixing and working conditions. We compared the obtained results to those published [24].

2.2.1. Flow domain

We designed a two-dimensional T-shaped rectangular microchannel (0.5 mm width and 8 mm length) with one inlet and two outlets using the SolidWorks software. We then imported the generated geometry to ANSYS Meshing 2020 R2. This program allowed us to generate a fine mesh of 21,846 quadrilateral cells and 22,612 nodes to allow accurate analysis of the simulation results.

2.2.2. Numerical model and validation

We analysed the trajectory of a single microparticle entering from the middle of the inlet along the channel using the DPM model, as in [24]. We defined the injection velocity as equal to the fluid velocity. We also applied a temperature gradient in the direction of the gravitational field, defining a lower temperature in the upper part of the microchannel and using the same conditions described in [24]. Table 1 shows the defined boundary conditions.

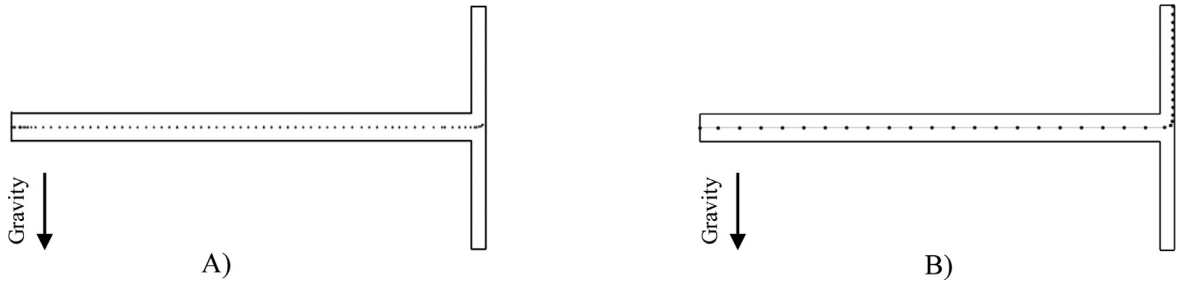

Fig. 1. Microparticle trajectory: Numerical results published by Eslamian et al. [24] A) and this work B).

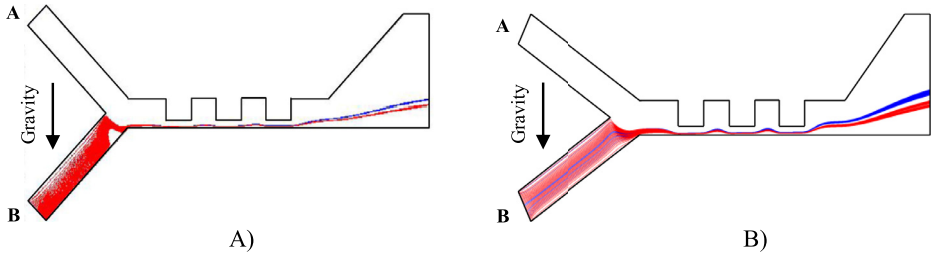

Fig. 2. Submicrometer particle separation. Numerical results published by Wang et al. [25] A) and this work B).

Table 2
Boundary conditions defined by Wang et al. [25].

Boundary	Type	Values
Inlet A	Velocity Inlet	$V = 2{\cdot}10^{-2}$ m/s
Inlet B	Velocity Inlet	$V = 2{\cdot}10^{-3}$ m/s $V_P = 2{\cdot}10^{-3}$ m/s
Outlet	Pressure Outlet Particle Scape	P gauge = 0 Pa
Hot wall (bottom part)	No-slip Particle Reflection	$T = 310$ K $e_n = 1.0$ (default)
Cold wall (upper part)	No-slip Particle Reflection	$T = 300$ K $e_n = 1.0$ (default)
Other walls	No-slip and Adiabatic Particle Reflection	$-k\nabla T = 0$ $e_n = 1.0$ (default)

We also specified the properties of the materials used in the simulations (water and PS particles). Note that we used the same density value of water for both the fluid and the PS microparticles, as was done in the work presented by Eslamian et al. [24]. We defined the magnitude of the thermodiffusion coefficient to be on the order of $1{\cdot}10^{-12}$ $m^2/s.K$ ($D_{T,i}$, Eq. (7)). In this way, we fulfilled the same working conditions as in [24].

The numerical results (Fig. 1) showed that the particle stream moves to the cold part of the channel exiting from the upper outlet. These results were consistent with those published by Eslamian et al. [24].

2.3. Case study 2: thermophoretic sorting of submicroparticles in an expansion-constriction microchannel

We investigated the thermophoretic force required to separate two groups of submicrometer-sized particles in an expansion-contraction microchannel. To do this, we performed a numerical simulation to analyse the migration of 0.5 and 1 μm particles suspended in water. We compared the obtained results to those published by Wang et al. [25].

2.3.1. Flow domain

We designed a two-dimensional sorter with an expansion-contraction channel composed of three main parts: two inlets; a separation channel (1.2 mm length and a maximum gap of 0.15 mm) that contains three orifices; and an enlarged output. As in the previous analysis, we used ANSYS Meshing 2020 R2 to define a fine mesh of the geometry for the subsequent numerical analysis. As in the previous case, we generated 21,846 quadrilateral cells and 22,612 nodes, as the channel has smaller dimensions the accuracy will be fine.

2.3.2. Numerical model and validation

We injected two groups of particles (0.5 and 1 μm) into inlet B (Fig. 2) using the DPM model. In this work, we defined two distinct injection velocities (inlet $A >$ inlet B). We also applied a temperature gradient parallel to the gravitational field, defining a lower temperature in the upper part of the microchannel, always with respect to the working conditions outlined in [25]. Table 2 shows the boundary conditions used.

We also specified the properties of the materials. We differentiated the density of the carrier fluid (998.2 kg/m^3) and particles (1040 kg/m^3) as described in [25]. We used the thermophoretic force ($2{\cdot}10^{-13}$ N) mentioned in [25,29] for both particle groups, and we estimated the order of magnitude of the thermodiffusion coefficient as $1{\cdot}10^{-10}$ $m^2/s{\cdot}K$ ($D_{T,i}$, Eq. (7)). After performing the numerical simulation, we observed a separation (Fig. 2) between the submicrometer particles (0.5 μm in blue and 1 μm in red). These results, again, are similar to those published by Wang et al. [25].

2.4. Results and discussion

The outcomes reported in Sections 2.2 and 2.3 confirm that we validated the results obtained in [24] and [25]. On the one hand, the work in [24] does not account for the difference in density between water and PS microparticles; for that reason, we repeated the numerical study. In this new analysis, we considered that the density of the microparticles is 1060 kg/m^3 [30] and that of water is 995.09 kg/m^3 (this work) at a temperature of 305 K. As shown

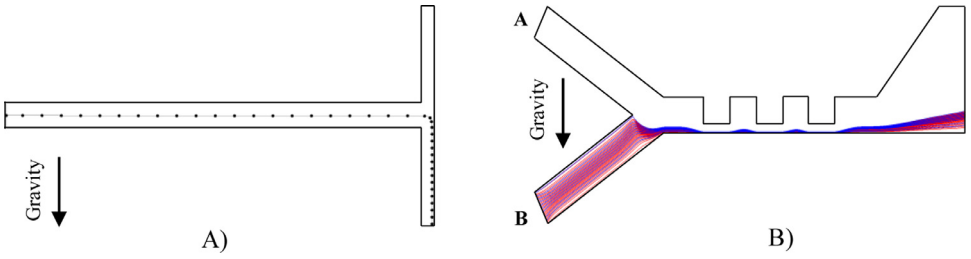

Fig. 3. The numerical model results: ρ_{water} = 995.09 kg/m^3 and $\rho_{particles}$ = 1060 kg/m^3 A) and $D_{T,i}$ = 1·10^{-12} m^2/s·K B).

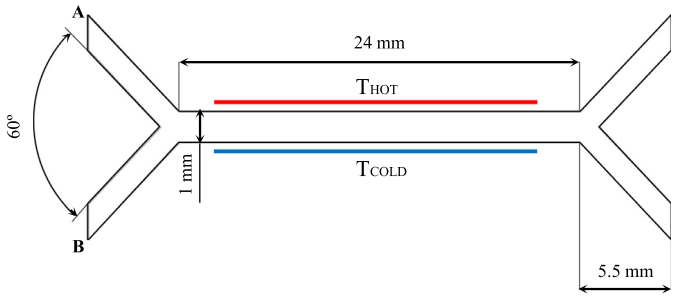

Fig. 4. Microchannel geometry to analyse the behaviour of microparticles in the presence of a positive thermal gradient.

in Fig. 3(A), the result is totally opposite to the one obtained in Fig. 1(B) and [24]. Specifically, the condition of the densities of the particles and that of the carrier fluid defined in [24] significantly affects the direction of particle motion. When the correct density values of PS and water are taken into account, the 1 µm particles always exit from the bottom outlet of the microchannel, regardless of the applied temperature gradient and position. Therefore, the gravity force is dominant.

On the other hand, in [25], a thermophoretic force of 2·10^{-13} N has been considered. This is equivalent to a thermodiffusion coefficient of the order of 1·10^{-10} m^2/s.K, an extremely higher magnitude than the ones shown in the literature (1·10^{-12} m^2/s.K) [31]. Therefore, we reanalysed the results achieved in [25], defining the thermodiffusion coefficient in this case in accordance with the bibliography. The obtained numerical results, shown in Fig. 3(B), demonstrate that the magnitude of the thermodiffusion coefficient directly affects the sorting of the particles, since no separation is achieved.

3. Size-based separation of polystyrene microparticles

Once we validated and analysed the two different studies to decide on an optimal numerical model, we designed a new microdispositive geometry for numerical and experimental analysis of the separation of two groups of PS microparticles in flow under a temperature gradient and in different configurations.

3.1. Numerical analysis

We designed a three-dimensional rectangular channel (1 mm width and 1 mm height) (Fig. 4) with two inlets and two outlets. Afterwards, for numerical simulations, as in the previous studies, we used the DPM model to calculate the trajectory of the particles along the central cavity.

We injected two different sizes of microparticles (5 and 20 µm) from the surface of inlet A at room temperature. The injection velocity of the particles was the same as that of the carrier fluid. We also used equal flow rates in both inlets. Regarding the physical properties, we considered the thermophoretic force using a thermodiffusion coefficient with an order of magnitude of 1·10^{-12} m^2/s·K ($D_{T,i}$, Eq. (7)) [31]. In addition, we defined the density value of the particles, together with the specific heat and thermal conductivity [30].

Apart from the aspects mentioned before, we specified various transport properties of the carrier fluid (water) necessary to perform the numerical analysis. In this work, we determined the principal characteristics, such as density, thermal expansion coefficient, dynamic viscosity, thermal conductivity and specific heat.

We carried out the measurement of the density and the thermal expansion coefficient using the Anton Paar DMA 5000 M vibrator-type densitometer with a U-form quartz tube sensor. We

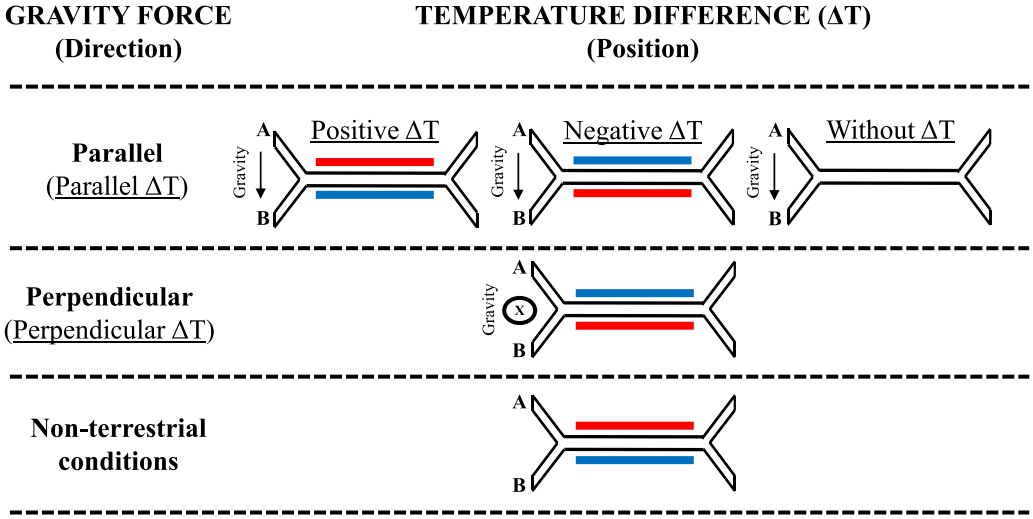

Fig. 5. Scheme of numerical cases resolved in this section.

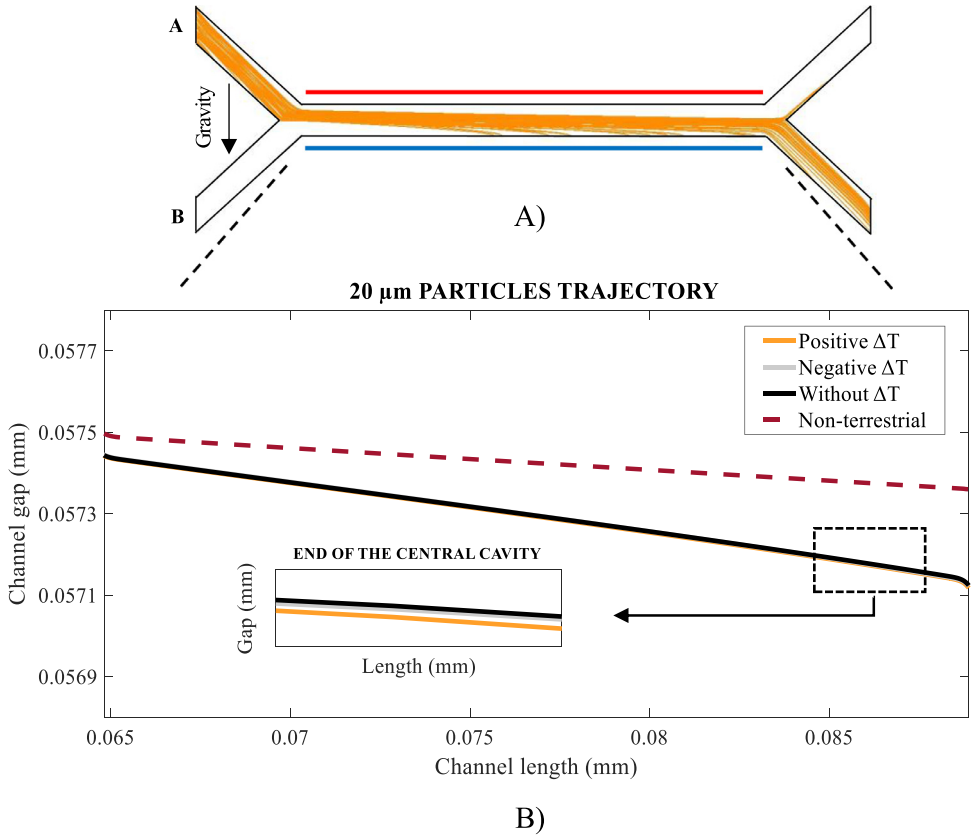

Fig. 6. A 20 µm particle path: along the microchannel A) and using different gradient positions together with zero gravity B).

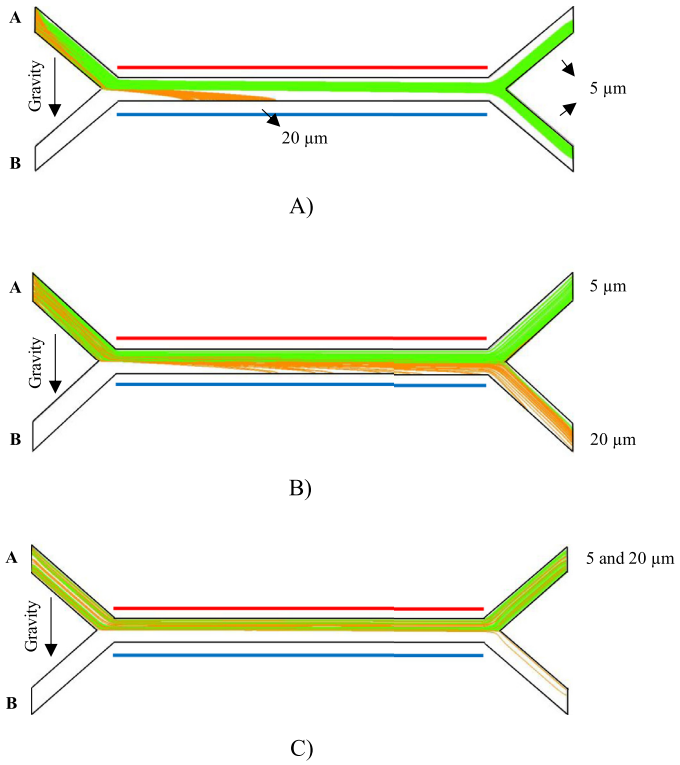

Fig. 7. 5 and 20 µm trajectory: flow rate = $1.5{\cdot}10^{-10}$ m^3/s A), flow rate = $6.8{\cdot}10^{-10}$ m^3/s B) and flow rate = $6.8{\cdot}10^{-9}$ m^3/s C).

determined the dynamic viscosity using an Anton Paar AMVn microviscometer and the falling ball principle. We also measured the thermal conductivity and specific heat of water using Thermtest THW-L1 equipment. In the case of the PS microparticles, we obtained all their properties from the literature. Table 3 summarises the defined characteristics.

We also defined the boundary conditions. As shown in Fig. 4, the flow domain consists of two inlets-outlets. In contrast to the previously analysed cases, we used mass-flow type inlets. We specified the other boundary condition types as in the previously studied models (Table 1 and Table 2).

In this section, we analysed different numerical cases (Fig. 5), taking into account the effect of the gravity force together with the temperature gradient position. To do this, we applied the gravitational field in a parallel or perpendicular direction to the temperature gradient. Additionally, we studied two more cases in which no gravity or temperature gradient was applied.

3.2. Numerical results

As mentioned before, we studied different cases to analyse both the thermodiffusion and the gravity effect in the separation of PS microparticles.

We first injected a single population of 20 µm from inlet A. We positioned the gravity force and the temperature gradient in the same direction, applying a lower temperature in the bottom part of the central cavity (Fig. 5 (Positive ΔT)). We specified a temperature difference of 10 K, together with a total flow rate of $6.8{\cdot}10^{-10}$ m^3/s. The obtained results, depicted in Fig. 6(A), show that the microparticles move towards the cold region of the channel and exit from the bottom part.

However, Fig. 6(B) shows that we obtained the same outcomes by not applying any temperature gradient (Fig. 6 (Without ΔT)) or

Table 3
Water and PS microparticle properties at 298.16 K.

Material	Water	PS Microparticles
Density (kg/m^3)	997.064 (this work)	1060 [30]
Specific heat (J/kg·K)	4021 (this work)	1220 [30]
Thermal conductivity (W/m·K)	0.60985 (this work)	0.11 [30]
Thermal expansion (K^{-1})	$2.5675 \cdot 10^{-4}$ (this work)	–
Viscosity (kg/m·s)	$8.7993 \cdot 10^{-4}$ (this work)	–
Thermodiffusion coefficient (m^2/s·K)	–	$1. \cdot 10^{-12}$ [31]

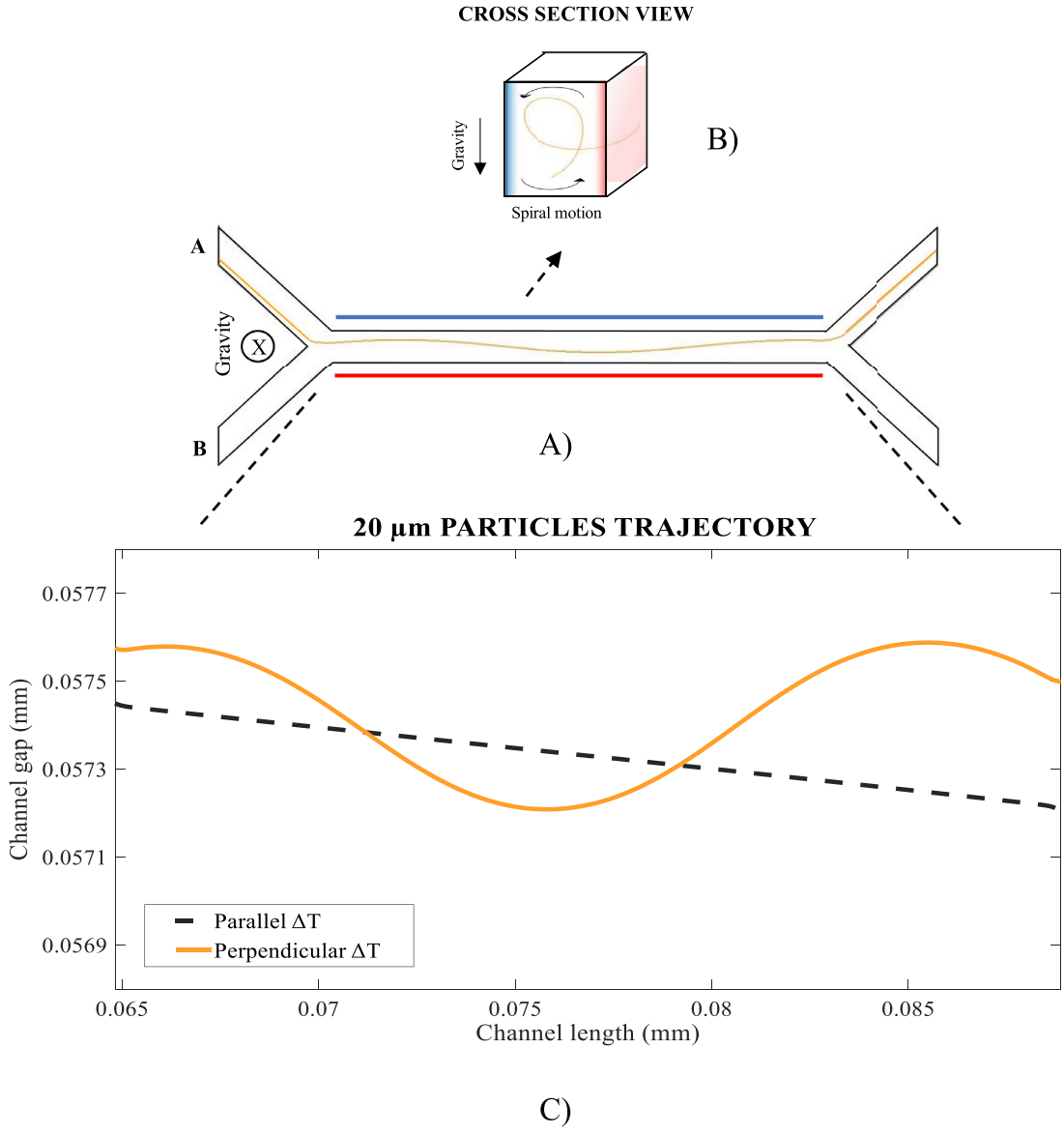

Fig. 8. Convection of 20 µm particles: along the microchannel A), showing the spiral motion in a cross-section view B) and comparing the direction of the gravitational field with respect to the temperature gradient C).

by positioning the cold region in the top part of the channel (Fig. 6 (Negative ΔT)).

We also analysed the condition of zero gravity (Fig. 5 (Non-terrestrial)). In this case, with a total flow rate of $6.8 \cdot 10^{-10}$ m^3/s, the 20 µm particles always exited from the top part of the microchannel, regardless of the applied thermal gradient (Positive ΔT, Negative ΔT or Without ΔT) due to the high flow rate used. For these working conditions, the results (Fig. 6(B)) show that the migration of the microparticles responds to the applied temperature gradient, as long as the initial flow rate is not higher than $1.36 \cdot 10^{-12}$ m^3/s. In the case of zero gravity, and using a defined temperature difference of (ΔT = 10 K), the magnitude of the PS microparticle migration depended on the applied flow rate; thus, the displacement to the cold wall was higher along the central channel when we defined smaller flow rates.

We also entered two groups of microparticles (5 and 20 µm) to evaluate the possibility of obtaining a separation of them at a total flow rate of $6.8 \cdot 10^{-10}$ m^3/s.

We analysed the separation process under three temperature gradient configurations (Positive ΔT, Negative ΔT and Without

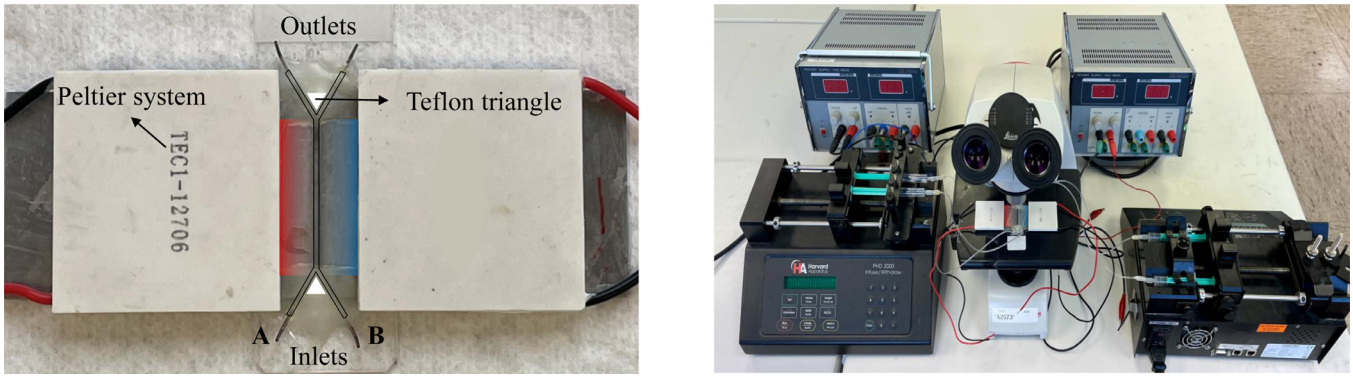

Fig. 9. On the left, the fabricated microdispositive. On the right, the experimental setup used.

ΔT). Fig. 7(B) shows the trajectory of the two groups of particles and that a separation was achieved due to the gravity effect, together with the applied flow rate conditions. The results always showed a migration of the 20 μm particles in the direction of the gravitational field, regardless of the temperature gradient used.

The separation between the microparticles was achieved based on the injection flow rate conditions, since the 20 μm species sedimented earlier due to the gravity force, whereas the 5 μm particles do not have time to sediment (total flow rate = $6.8{\cdot}10^{-10}$ m^3/s) under these conditions. We demonstrated that using higher flow rates (of the order of $6.8{\cdot}10^{-9}$ m^3/s) caused almost all the microparticles to exit from the top outlet (**Fig. 7**(C)). Smaller flow rates (of the order of $1.5{\cdot}10^{-10}$ m^3/s) caused the 20 μm particles to sediment completely and the 5 μm particles started to exit from the bottom outlet (**Fig. 7**(A)) regardless of the thermal gradient used.

We studied another case by injecting a single population of 20 μm particles and positioning the temperature gradient in a direction perpendicular to the gravity field. The boundary conditions (total flow rate = $6.8.10^{-10}$ m^3/s and temperature difference = 10 K) were otherwise the same as in the previous numerical cases. The results (Fig. 8) showed a spiral motion of the particles throughout the central cavity.

This convection generated due to the thermogravitational effect caused the particles to move constantly in one section of the channel (Fig. 8(B)), dictated by the sum of the effect of the temperature gradient (horizontal displacement of particles) together with the gravitational field (vertical displacement) and the drag effect generated by the applied inlet flow rate. The sum of these three effects made it difficult to control the particle migration.

4. Experimental validation

We validated the numerical results of the gravitational effect on the separation of the microparticles under the different configurations by analysing the same cases experimentally.

We first fabricated a microdevice (Fig. 9) with similar dimensions to the one analysed numerically. We used two aluminium plates for the central cavity, together with two Teflon triangles (side dimensions = 1 mm and angle = 60°), to generate the path of the inlets and outlets of the microdevice and to isolate from the temperature gradient. We selected aluminium material for the walls where the temperature gradient is applied due to its good conductivity properties. We also used glass plates to seal the microdevice, as this allowed visualisation of its interior.

To generate the desired flow rates, we connected the inputs and outputs of the microdispositive via microfluidic tubes to a HARVARD PHD 2000 Infusion/Withdraw pump, as shown in Fig. 9.

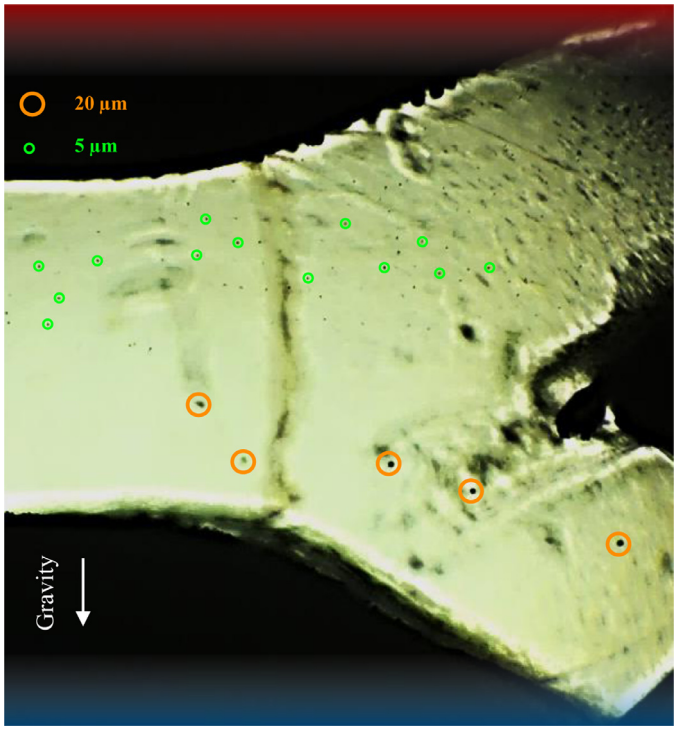

Fig. 10. Experimental validation: separation of PS microparticles (5 μm and 20 μm).

We generated the temperature gradient with a Peltier system connected to a power supply, measuring and monitoring the temperature in the aluminium plates by means of PT-100 thermocouples. We also used a Leica DM500 binocular microscope to visualise and record the trajectory of the injected particles.

As in the studied numerical cases, we distinguished two main conditions by applying the temperature gradient in a parallel or perpendicular direction to the gravitational field. In this way, we analysed the separation of the microparticles and evaluated the effect of the gravity force for each of the conditions.

In all the experiments, we defined the same initial conditions as in the numerical simulations (ΔT = 10 K and total flow rate = $6.8{\cdot}10^{-10}$ m^3/s). After analysing all the possible configurations shown in Fig. 5, the results obtained in every case showed that the effect of the temperature gradient is absolutely null and the gravity force is dominant in all the analysed conditions.

We analysed the separation of two groups of microparticles (5 μm and 20 μm) in water with the mentioned flow rate and at different ΔT configurations (Positive, Negative and Without). We

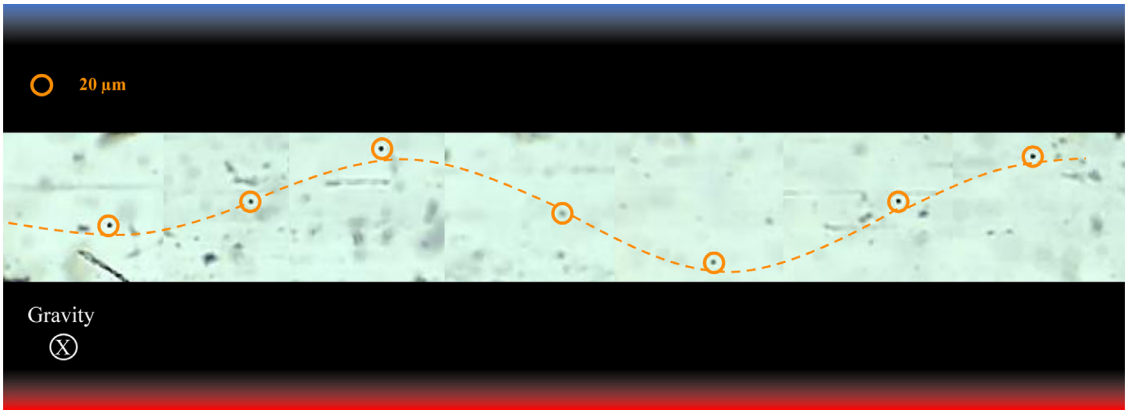

Fig. 11. Experimental validation: convection of PS microparticles.

obtained identical results to those showed in Fig. 7(B), regardless of the effect of the temperature gradient. Fig. 10 shows the experimental separation of two groups of microparticles when applying a temperature gradient of 10 K and a total flow rate of $6.8{\cdot}10^{-10}$ m^3/s.

For the case in which the applied temperature gradient is perpendicular to the gravitational field, we observed experimentally the same phenomenon that we had analysed numerically (Fig. 8). We injected a group of 20 µm and, as shown in Fig. 11, we saw a convective displacement of the microspheres along the central cavity due to the combination of the thermogravitational effect together with the applied flow rate.

5. Conclusions

The main objective of this work was to analyse the potential use of the thermodiffusion phenomenon for the separation of PS microparticles in microfluidic devices.

We demonstrated numerically and experimentally that the phenomenon of thermodiffusion is not valid as an application in separation processes for particles of 5 µm and larger in flow under the analysed working conditions and with the fabricated microdevice geometry. We concluded that the gravity effect overcomes the thermodiffusion phenomenon in all studied cases. In parallel, the numerical results indicated that ANSYS Fluent is an appropriate software for simulating the separation of binary mixtures and molecular suspensions. We also showed the importance of not neglecting the small differences in density between fluid (water in that case) and PS microparticles, as was done in [24], and of not overestimating the magnitude of the thermodiffusion coefficient, as in [25].

We observed the thermogravitational effect when a perpendicular temperature gradient was applied in the central channel of the microdevice. This phenomenon can be useful in microfluidics for optimising the mixing of different fluids. A higher temperature gradient and a lower total flow rate generated a major convection of the flow along the channel.

Our future studies will focus on numerical and experimental analyses of the thermodiffusion phenomenon for PS nanoparticles separation. Gravity is not expected to have as great an effect on nanosized versus microsized particles, as thermodiffusion becomes the main force driving the separation of different groups of nanoparticles.

Declaration of competing interest

The authors declare no competing financial interest.

CRediT authorship contribution statement

Antton Sanjuan: Conceptualization, Methodology, Software, Validation, Formal analysis, Investigation, Data curation, Writing – original draft, Writing – review & editing. **Ane Errarte:** Conceptualization, Formal analysis, Writing – review & editing. **M. Mounir Bou-Ali:** Conceptualization, Methodology, Data curation, Resources, Writing – review & editing, Supervision, Project administration, Funding acquisition.

6. Acknowledgements

The present work has been supported by KK-2021/00082 (micro4IloT), IT1505–22 (Research Group Program) and PRE-2019–1–0202 of the Basque Government and PID2020–115086GB-C33 financed by MCIN/AEI of the Spanish Government.

References

[1] C. Ludwig, Diffusion zwischen ungleich erwärmten Orten gleich zusammengesetzter Lösungen, Sitz. Ber. Akad. Wiss. Wien Math-Naturw 20 (1856) 539.
[2] C. Soret, Au Point De Vue De Sa Concentration une Dissolution Saline Primitevement Homogéne Dont Deux Parties Sont Portées a Des Temepératures Différentes, Arch. des Sci. Phys. Nat. Genéve 3 (1879) 48–61.
[3] W. Köhler, K.I.K.I. M.orozov, The soret effect in liquid mixtures - a review, J. Non-Equilibrium Thermodyn. 41 (3) (2016) 151–197, doi:10.1515/jnet-2016-0024.
[4] D.E.D.E. R.osner, Thermal (Soret) diffusion effects on interfacial mass transport rates, Phys. Chem. Hydrodyn. 1 (2) (1960) 1858–1864.
[5] J. Schott, Thermal diffusion and magmatic differentiation : a new look at an old problem, Bull. Minéralogie 106 (1) (1983) 247–262, doi:10.3406/bulmi.1983.7685.
[6] F. Montel, Importance de la Thermdiffusion en Exploracion et production Pétrolières, Entropie 184/185 (1994) 86–93.
[7] D. Braun, A. Libchaber, Trapping of DNA by Thermophoretic depletion and convection, Phys. Rev. Lett. 89 (18) (Oct. 2002) 188103, doi:10.1103/PhysRevLett.89.188103.
[8] A. Martin, M.M.M.M. B.ou-Ali, H. Barrutia, D. Alonso de Mezquia, Microfluidic separation process by the soret effect in biological fluids, Comptes Rendus Mécanique 339 (5) (May 2011) 342–348, doi:10.1016/j.crme.2011.03.012.
[9] A. Martin-Mayor, M.M.M.M. B.ou-Ali, M. Aginagalde, P. Urteaga, Microfluidic separation processes using the thermodiffusion effect, Int. J. Therm. Sci. 124 (Feb. 2018) 279–287, doi:10.1016/j.ijthermalsci.2017.10.024.
[10] F.J.F.J. B.onner, L.-.O. Sundelöf, Thermal diffusion as a mechanism for biological transport, Zeitschrift für Naturforsch. C 39 (6) (Jun. 1984) 656–661, doi:10.1515/znc-1984-0623.
[11] D. Braun, A. Libchaber, Thermal force approach to molecular evolution, Phys. Biol. 1 (1) (Mar. 2004) P1–P8, doi:10.1088/1478-3967/1/1/P01.
[12] A. Martin, M.M.M.M. B.ou-Ali, Determination of thermal diffusion coefficient of Nanofluid: fullerene–Toluene, Comptes Rendus Mécanique 339 (5) (May 2011) 329–334, doi:10.1016/j.crme.2011.03.010.
[13] D. Niether, D. Afanasenkau, J.K.J.K.G. Dhont, S. Wiegand, Accumulation of formamide in hydrothermal pores to form prebiotic nucleobases, Proc. Natl. Acad. Sci. 113 (16) (Apr. 2016) 4272–4277, doi:10.1073/pnas.1600275113.
[14] D. Niether, M. Sarter, B.W.B.W. K.oenig, J. Fitter, A.M.A.M. S.tadler, S. Wiegand, Thermophoresis: the case of streptavidin and biotin, Polymers (Basel) 12 (2) (Feb. 2020) 376, doi:10.3390/polym12020376.

[15] A. Bahat, M. Eisenbach, Sperm thermotaxis, Mol. Cell. Endocrinol. 252 (1–2) (Jun. 2006) 115–119, doi:10.1016/j.mce.2006.03.027.
[16] L.H.L.H. T.hamdrup, N.B.N.B. L.arsen, A. Kristensen, Light-induced local heating for Thermophoretic manipulation of DNA in polymer Micro- and Nanochannels, Nano Lett 10 (3) (Mar. 2010) 826–832, doi:10.1021/nl903190q.
[17] N. Lee, S. Wiegand, Thermophoretic micron-scale devices: practical approach and review, Entropy 22 (9) (Aug. 2020) 950, doi:10.3390/e22090950.
[18] R. Piazza, A. Parola, Thermophoresis in colloidal suspensions, J. Phys. Condens. Matter 20 (15) (Apr. 2008) 153102, doi:10.1088/0953-8984/20/15/153102.
[19] A. Errarte, et al., Thermophoresis as a technique for separation of nanoparticle species in microfluidic devices, Int. J. Therm. Sci. 156 (Oct. 2020) 106435, doi:10.1016/j.ijthermalsci.2020.106435.
[20] S. Ramachandran, C.B.C.B. S.obhan, G.P.G.P. P.eterson, Thermophoresis of nanoparticles in liquids, Int. J. Heat Mass Transf. 147 (Feb. 2020) 118925, doi:10.1016/j.ijheatmasstransfer.2019.118925.
[21] S. Panesar, S. Neethirajan, Microfluidics: rapid diagnosis for breast cancer, Nano-Micro Lett 8 (3) (Jul. 2016) 204–220, doi:10.1007/s40820-015-0079-8.
[22] J.K.J.K. P.latten, The soret effect: a review of recent experimental results, J. Appl. Mech. Trans. ASME 73 (1) (2006) 5–15, doi:10.1115/1.1992517.
[23] R. Piazza, Thermophoresis: moving particles with thermal gradients, Soft Matter 4 (9) (2008) 1740, doi:10.1039/b805888c.
[24] M. Eslamian, M.Z.M.Z. S.aghir, Novel Thermophoretic Particle Separators: numerical Analysis and Simulation, Appl. Therm. Eng. 59 (1–2) (Sep. 2013) 527–534, doi:10.1016/j.applthermaleng.2013.06.020.
[25] R. Wang, S. Sun, W. Wang, Z. Zhu, Investigation on the Thermophoretic sorting for Submicroparticles in a sorter with expansion-contraction microchannel, Int. J. Heat Mass Transf. 133 (Apr. 2019) 912–919, doi:10.1016/j.ijheatmasstransfer.2018.12.126.
[26] T.D.T.D. C.anonsburg, ANSYS FLUENT User's Guide, [Online] (2013) 2692 Available http://www.pmt.usp.br/academic/martoran/notasmodelosgrad/ANSYSFluentUsersGuide.pdf .
[27] T.D.T.D. C.anonsburg, ANSYS fluent theory guide, [Online] (2013) 814 Available http://www.pmt.usp.br/academic/martoran/notasmodelosgrad/ANSYSFluentTheoryGuide15.pdf .
[28] H. Ounis, G. Ahmadi, J.B.J.B. M.cLaughlin, Brownian diffusion of Submicrometer particles in the viscous sublayer, J. Colloid Interface Sci. 143 (1) (Apr. 1991) 266–277, doi:10.1016/0021-9797(91)90458-K.
[29] R. Wang, J. Du, W. Guo, Z. Zhu, Investigation on the thermophoresis-coupled inertial sorting of Submicrometer particles in a microchannel, Nanoscale Microscale Thermophys. Eng. 20 (1) (Jan. 2016) 51–65, doi:10.1080/15567265.2015.1124159.
[30] J. Wiley, Polymer Handbook, 2nd ed., 1975 New York.
[31] M. Braibanti, D. Vigolo, R. Piazza, Does Thermophoretic mobility depend on particle size? Phys. Rev. Lett. 100 (10) (Mar. 2008) 108303, doi:10.1103/PhysRevLett.100.108303.